

Journal of Biomedical Optics

BiomedicalOptics.SPIEDigitalLibrary.org

Simultaneous measurement of refractive index and thickness of multilayer systems using Fourier domain optical coherence tomography, part 1: theory

Payman Rajai
Henry Schriemer
Ahmad Amjadi
Rejean Munger

SPIE.

Payman Rajai, Henry Schriemer, Ahmad Amjadi, Rejean Munger, "Simultaneous measurement of refractive index and thickness of multilayer systems using Fourier domain optical coherence tomography, part 1: theory," *J. Biomed. Opt.* **22**(1), 015002 (2017), doi: 10.1117/1.JBO.22.1.015002.

Simultaneous measurement of refractive index and thickness of multilayer systems using Fourier domain optical coherence tomography, part 1: theory

Payman Rajai,^{a,*} Henry Schriemer,^{a,b} Ahmad Amjadi,^c and Rejean Munger^a

^aUniversity of Ottawa, Physics Department, 150 Louis Pasteur, Ottawa, Ontario K1N 6N5, Canada

^bUniversity of Ottawa, School of Electrical Engineering and Computer Science, Ottawa, Ontario K1N 6N5, Canada

^cSharif University of Technology, Physics Department, P.O. Box: 11155-9161, Tehran, Iran

Abstract. We introduce a theoretical framework for simultaneous refractive index and thickness measurement of multilayer systems using the Fourier domain optical coherence tomography (FD-OCT) system without any previous information about the item under investigation. The input data to the new formalism are the FD-OCT measured optical path lengths and properly selected spectral components of the FD-OCT interference spectrum. No additional arrangement, reference reflector, or mechanical scanning is needed in this approach. Simulation results show that the accuracy of the extracted parameters depends on the index contrast of the sample while it is insensitive to the sample's thickness profile. For transparent biological samples with smooth interfaces, when the object is in an aqueous medium and has indices <1.55 , this method can extract indices and thicknesses with the absolute error ≤ 0.001 . © 2017 Society of Photo-Optical Instrumentation Engineers (SPIE) [DOI: [10.1117/1.JBO.22.1.015002](https://doi.org/10.1117/1.JBO.22.1.015002)]

Keywords: optical coherence tomography; Fourier domain; refractive index; multilayer systems.

Paper 160711R received Oct. 17, 2016; accepted for publication Jan. 3, 2017; published online Jan. 28, 2017.

1 Introduction

Optical coherence tomography (OCT) is a noninvasive interferometric imaging technique that provides high-resolution morphological cross-sectional information, thus enabling the three-dimensional (3-D) reconstruction of the reflectivity profile of structures. In the last decade, OCT has become a pervasive imaging technology with particular application in ophthalmology as a standard tool for diagnosis and monitoring of several ocular diseases.¹ The first generation OCT system, called time-domain OCT (TD-OCT), was based on mechanically scanning a reference mirror to measure the time-of-flight of the optical signal reflected from the sample.² Another main category of OCT systems is Fourier-domain OCT (FD-OCT) whereby the reference arm is fixed and the detection system is replaced with a spectrometer. The internal structure of the object is then revealed by Fourier transform of the interference spectrum between the reference and sample arms fields.³ FD-OCT dramatically improves the detection sensitivity and enables significantly higher scan speeds than earlier TD-OCT.^{4–6} Current implementations of OCT imaging can provide only the optical path length between reflecting structures. In order to extract the optical properties and the true structure size of the object under investigation, separation of refractive index and thickness from the OCT-measured optical paths is needed.

The ability to noninvasively measure both refractive index and thickness of biological tissues could have broad medical applications. In optical diagnostics, monitoring changes in refractive index can help distinguish between tissue with normal or abnormal function, thus enabling earlier disease detection.⁷ For example, in ophthalmology, accurate knowledge of the cornea refractive index and thickness can help to improve the outcome of surgical procedures while they are indicators of cornea states of

hydration and intraocular pressure.⁸ Also, the retina layers profile is linked to diseases like glaucoma,⁹ diabetes,¹⁰ and several neuro-ophthalmic diseases like Alzheimer's, Parkinson's, and multiple sclerosis.¹¹ Therefore, accurate measurement of the retina layers true thickness and refractive index profile can help for early diagnosis and prognosis of the diseases. Other applications can be found in brain tumor,¹² breast cancer,¹³ etc.

Several techniques have been reported for simultaneous measurement of refractive index and thickness using an OCT system in both TD and FD. These techniques suitable for single layer objects can be listed in TD as low-coherence reflectometry,^{14–18} focus-tracking method,^{19–29} bifocal optical coherence refractometry,^{30,31} digital refocusing technique,^{32,33} and tandem configuration of interferometers for dispersion-insensitive measurements.^{34–36} In the FD approach, the simultaneous measurement of refractive index and thickness of a single layer object has been reported using a reference plane behind the object,^{37,38} providing a step on the object,³⁹ using a dual sample probe⁴⁰ or by fitting a modeled signal to the actual spectrum.⁴¹

For more than one-layer objects, the focus-tracking technique has been used to measure the refractive index and thickness of two- and three-layer systems (the cornea)^{42,43} and three layers of the skin.⁴⁴ This technique employs low-coherence interferometry combined with the translation of the focus of an objective lens inside biological tissues. The measurement accuracy of this method is usually limited by the resolution of translation stages (moving the focus point or the sample) installed in the system. Also, the FD approach has been used for three-layer silica-crown-dental composite-silica structure.^{45,46} In the proposed method, the real spectral data are fitted to a modeled signal spectrum searching for index and thickness. A computer program searches for a wide range of possible index and thickness

*Address all correspondence to: Payman Rajai, E-mail: paymanrajai@gmail.com

combinations, using the optical path length of each layer as constraints until the best fit is achieved. This approach is purely a fitting process without measuring index and thickness.

In the search for a new approach, in this article, we first show that under assumptions consistent with FD-OCT technology, there is a theoretical framework for the analysis of spectral OCT data that decouples the index of refraction and thickness information in stratified media without needing any previous information about the item under investigation. We use computer simulation to implement the methodology associated with the new framework. Our simulated experimental FD-OCT signal will be generated using the transfer matrix method. We then investigate the relationship between the accuracy of this framework and the built-in assumptions for a range of multilayer cases simulating real-world applications.

For simplicity and without losing the generality, we use the new framework to extract two-layer system parameters. These parameters are refractive index and thickness of the layers and the last medium index of refraction. We test the methodology for a range of sample's thickness and index contrast, searching for any systematic dependence of the extracted parameter errors with respect to sample's index and thickness profile.

2 Method

We start with the basic FD-OCT geometry, depicted in Fig. 1, where the field amplitude of the beam from a short coherent light source is divided into two beams, one incident on a reference mirror and one incident on the object. We assume a stratified object with ideally flat interfaces. We also assume that the object is nonabsorbing, isotropic, and homogeneous in refractive index. The fields reflected from the object and reference mirror are recombined onto a spectrometer. We model the spectrometer signal using the simple but often used summation method, which assumes that the field components arising from multiple scattering between interfaces (multiple reflections) inside the object are negligible. This approximation is valid for biological samples.⁴⁷

At the beam splitter, the field reflected from the reference mirror has traveled a round trip distance of $2Z_R$ and can be given as follows:

$$U^R(k) = r_{(R)}s(k)\exp(i2kZ_R), \quad (1)$$

where k is the wavenumber, $s(k)$ is the source spectral amplitude, and $r_{(R)}$ represents the reflectivity of the reference mirror,

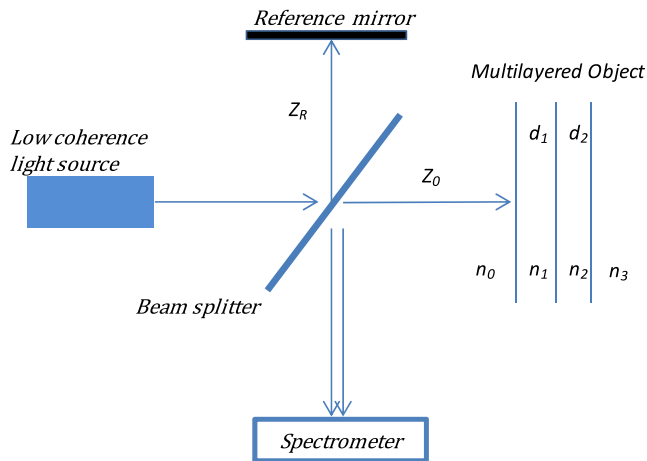


Fig. 1 Schematic presentation of the FD-OCT system. $\{n_i, d_i\}$ represent the index and thickness of each layer of the sample.

assuming to be unity. The total field reflected from the object at the beam splitter position is the sum of the fields reflected from each interface:⁴⁵

$$U^s(k) = s(k) \sum_1^{N+1} r_{(j)} \exp\left(i2k \sum_{l=0}^j n_l d_l\right), \quad (2)$$

where k is the wavenumber in free space, N is the number of layers, n_l and d_l are the refractive index and the physical thickness of the l 'th layer ($n_0 d_0 = Z_0$), and $r_{(j)}$ is the field amplitude reflected from each interface. The reflected field amplitude depends on the incident field amplitude on the interface. For low refractive index contrast, we can make the approximation that the incident signal on each interface is the same and the reflected field amplitude $r_{(j)}$ is the Fresnel coefficient.

The detected signal intensity by the detector after interference between the two-arm fields is as follows:

$$I^{\text{SUM}}(k) = |U^R + U^s|^2. \quad (3)$$

For a two-layer system, Eq. (3) takes the form:⁴⁷

$$\begin{aligned} I^{\text{SUM}}(k) = & S(k)(1 + r_{(1)}^2 + r_{(2)}^2 + r_{(3)}^2) \\ & + 2S(k)\{r_{(1)}r_{(2)} \cos(2k\delta_1) + r_{(1)}r_{(3)} \cos[2k(\delta_1 + \delta_2)] \\ & + r_{(2)}r_{(3)} \cos(2k\delta_2)\} + 2S(k)\{r_{(1)} \cos(2k\Delta_{Z_R Z_0}) \\ & + r_{(2)} \cos[2k(\Delta_{Z_R Z_0} - \delta_1)] + r_{(3)} \cos[2k(\Delta_{Z_R Z_0} - \delta_1 - \delta_2)]\}, \end{aligned} \quad (4)$$

where $S(k)$ is the source power spectral density, $\Delta_{Z_R Z_0} = Z_R - Z_0 \leq 0$ is the mismatch in arm's length, and δ_1, δ_2 are the optical path lengths of each layer. The right-hand side of Eq. (4) contains three groups of terms: the first term is a constant offset (DC), the second is an autocorrelation (AC), and the third is a cross-correlation terms. In the conventional FD-OCT system, the DC and AC terms are considered unwanted terms and can be removed by phase-shifting interferometry.⁴⁸ The normalized spectral response of the detector, $I(k)$, after removing the DC and AC terms is as follows:

$$\begin{aligned} I(k) = & \frac{I^{\text{SUM}}(k) - DC - AC}{2S(k)} \\ = & r_{(1)} \cos(2k\Delta_{Z_R Z_0}) + r_{(2)} \cos[2k(\Delta_{Z_R Z_0} - \delta_1)] \\ & + r_{(3)} \cos[2k(\Delta_{Z_R Z_0} - \delta_1 - \delta_2)]. \end{aligned} \quad (5)$$

In our new approach, we first obtain the optical path length of each layer (δ_1, δ_2), the usual output from a conventional FD-OCT obtained from the Fourier transform of the interference spectrum. When this information is fed back into $I(k)$ in Eq. (5), the only unknowns left are the Fresnel coefficients. For a two-layer system with three interfaces, there are three Fresnel coefficients to be calculated. We may find three appropriate values of $k(k_1, k_2, k_3)$, such that their application in Eq. (5) gives three linearly independent equations. The Fresnel coefficients can be found from the following matrix equation:

$$\begin{pmatrix} r_{(1)} \\ r_{(2)} \\ r_{(3)} \end{pmatrix} = (P)^{-1} \cdot \begin{pmatrix} I(k_1) \\ I(k_2) \\ I(k_3) \end{pmatrix}, \quad (6)$$

where

$$(P) = \begin{pmatrix} \cos(2k_1 \Delta_{ZR} Z_0) & \cos[2k_1 (\Delta_{ZR} Z_0 - \delta_1)] & \cos[2k_1 (\Delta_{ZR} Z_0 - \delta_1 - \delta_2)] \\ \cos(2k_2 \Delta_{ZR} Z_0) & \cos[2k_2 (\Delta_{ZR} Z_0 - \delta_1)] & \cos[2k_2 (\Delta_{ZR} Z_0 - \delta_1 - \delta_2)] \\ \cos(2k_3 \Delta_{ZR} Z_0) & \cos[2k_3 (\Delta_{ZR} Z_0 - \delta_1)] & \cos[2k_3 (\Delta_{ZR} Z_0 - \delta_1 - \delta_2)] \end{pmatrix}. \quad (7)$$

Not all sets of spectral components can be used to solve Eq. (6) since for some sets, the matrix (P) is singular, as the chosen wavenumber components provide the same phase information from the interfaces. The description of the determinant's roots can be found in reference.⁴⁹ Once the Fresnel coefficients are found, the required refractive index may then be extracted directly from the Fresnel coefficients, if n_0 is known, using

$$r_{(j)} = \frac{n_{j-1} - n_j}{n_{j-1} + n_j}, \quad j = 1, 2, 3, \quad (8)$$

and thickness of each layer can be extracted then from

$$d_{1,2} = \frac{\delta_{1,2}}{n_{1,2}}. \quad (9)$$

In summary, we extract both refractive index and thickness by

1. obtaining the normalized spectrum free from DC and AC terms [Eq. (5)],

2. extracting the optical thickness from the Fourier transform of Eq. (5),
3. selecting appropriate wavenumber components,
4. constructing the matrix equation, Eq. (6),
5. extracting indices from the Fresnel coefficients [Eq. (8)],
6. extracting layer thicknesses from Eq. (9).

It is worth noting that Eq. (6) can be generalized to any multi-layer systems. An N -layer system has $N + 1$ interfaces; therefore, we need $N + 1$ spectral components to calculate $N + 1$ Fresnel coefficients, so we have

$$\begin{pmatrix} r_{(1)} \\ r_{(2)} \\ \vdots \\ r_{(N+1)} \end{pmatrix} = (P)^{-1} \begin{pmatrix} I(k_1) \\ I(k_2) \\ \vdots \\ I(k_{N+1}) \end{pmatrix}, \quad (10)$$

where the matrix is

$$P = \begin{pmatrix} \cos(2k_1 \Delta_{ZR} Z_0) & \cos[2k_1 (\Delta_{ZR} Z_0 - \delta_1)] & \cdots & \cos \left[2k_1 \left(\Delta_{ZR} Z_0 - \sum_{i=1}^N \delta_i \right) \right] \\ \cos(2k_2 \Delta_{ZR} Z_0) & \cos[2k_2 (\Delta_{ZR} Z_0 - \delta_1)] & \cdots & \cos \left[2k_2 \left(\Delta_{ZR} Z_0 - \sum_{i=1}^N \delta_i \right) \right] \\ \vdots & \vdots & \ddots & \vdots \\ \cos(2k_{N+1} \Delta_{ZR} Z_0) & \cos[2k_{N+1} (\Delta_{ZR} Z_0 - \delta_1)] & \cdots & \cos \left[2k_{N+1} \left(\Delta_{ZR} Z_0 - \sum_{i=1}^N \delta_i \right) \right] \end{pmatrix}. \quad (11)$$

3 Results

In this section, we test the applicability of the introduced index-thickness measurement method for specific system realizations against digitally constructed test data. A realistic FD-OCT signal will be generated using the transfer matrix method to simulate real life data acquisition. We will use the new formalism to extract two-layer system parameters (i.e., n_1, n_2, n_3, d_1, d_2) to validate the new framework in a perfect situation when the error in optical thickness measurement is negligible ($\varepsilon = 0$). We will test the new methodology for a wide range of index contrasts and thickness of two-layer systems to determine if there is any systematic dependence of the "error" (the difference between actual parameters and extracted parameters) with respect to index contrast and thickness. Although there might be applications for the work presented in this article outside of the OCT framework, the work presented here is focused on biological applications of OCT. The more realistic situation when $\varepsilon \neq 0$ will be discussed in the next section.

3.1 Impact of Refractive Index Profile

As discussed previously on the summation method, the main constraint on our index-thickness extraction method is that

the Fresnel coefficients be small, meaning that the indices difference across an interface (index contrast) be small. As the contrast increases, multiple reflections are no longer negligible and hence, the summation method is not sufficient to describe the reflected spectrum accurately. This induces error in the sample's extracted parameters using the matrix formulation [Eq. (6)].

To illustrate the impact of refractive index profile on the extracted parameters for biological applications, we assume that a two-layer system is immersed into an aquatic medium with index of refraction 1.337. The extracted parameters error distribution map is provided for a range of n_1 and n_2 from 1.337 to 1.90 in 0.11 increments while $n_3 = 1.337$ but must be estimated by the program. Both thicknesses are set to $30 \mu\text{m}$ and a total of 2600 test models were thus tested. In Fig. 2, the horizontal axis corresponds to the actual n_1 value and the vertical axis corresponds to the actual n_2 value in the models tested, and the color map is the extracted parameter error. The irregularities appearing on the top right and the narrow band on the bottom of the figure correspond to the models that their optical thicknesses could not be determined correctly by the FD-OCT simulation program due to very large refractive index contrast ratio between the interfaces.

The error distribution in $n_1:n_2$ space for n_1 in Fig. 2(a) shows that for $n_1 < 1.55$, the absolute error is consistently

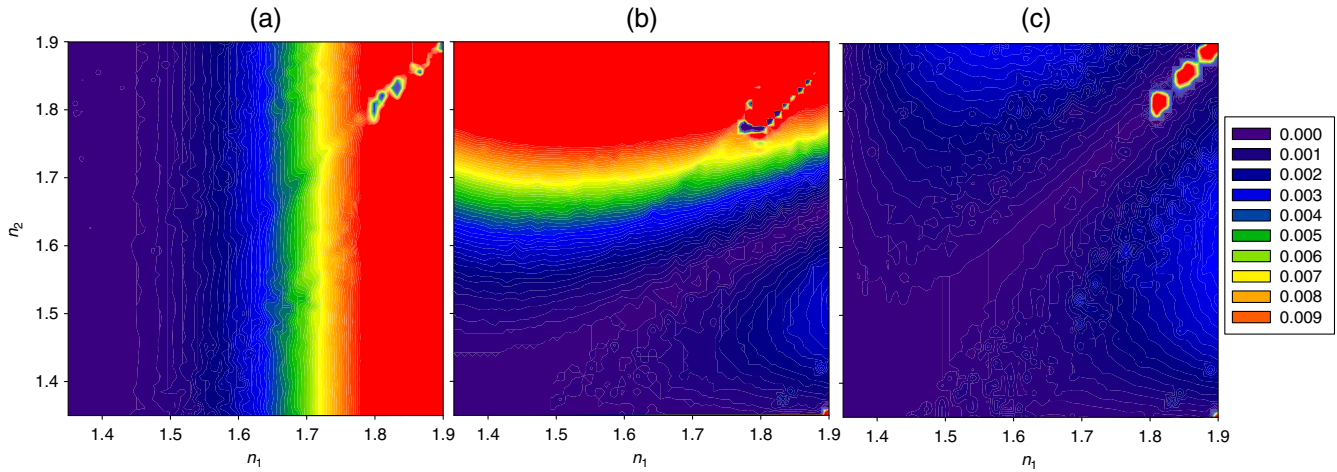


Fig. 2 The contour map corresponding to the absolute error distribution of the extracted (a) n_1 , (b) n_2 , and (c) n_3 . The horizontal axis corresponds to varying n_1 and the vertical axis corresponds to varying n_2 . The region with the absolute error ≤ 0.001 for all indices is limited to test models with $n_{1,2} \leq 1.55$.

less than 0.001, an area of interest as it is more desirable for biological applications. The region with the same accuracy for n_2 , Fig. 2(b), is roughly restricted to $n_1 < 1.75$ and $n_2 < 1.55$ and for n_3 , in Fig. 2(c), is limited to the region with $n_1 < 1.70$ and $n_2 < 1.70$. From Fig. 2, we may conclude that n_1 , n_2 , and n_3 can be extracted with the absolute error ≤ 0.001 for those test models having both $n_{1,2} \leq 1.55$.

The relative error distribution of the extracted thicknesses follows almost the same pattern of the corresponding index since from Eq. (9), we have

$$\frac{\Delta d_{1,2}}{d_{1,2}} = \pm \sqrt{\left(\frac{\Delta \delta_{1,2}}{\delta_{1,2}}\right)^2 + \left(\frac{\Delta n_{1,2}}{n_{1,2}}\right)^2}. \quad (12)$$

3.2 Impact of Sample Thickness

The impact of the sample thickness on extracting the parameters is evaluated in this section. We consider a two-layer test model with $n_0 = 1.337$, $n_1 = 1.345$, $n_2 = 1.351$, and $n_3 = 1.337$. The

thickness of the first layer is fixed at $30 \mu\text{m}$ and the thickness of the second layer varies from $30 \mu\text{m}$ up to $1580 \mu\text{m}$, which is the maximum detectable range of our FD-OCT simulation system with $20 \mu\text{m}$ increments. The parameters to be extracted are the index and thickness of each layer and the last medium index of refraction. The test result is shown in Fig. 3, where the vertical axis is the error in the extracted parameters and the horizontal axis is the varying thickness. In this figure, the left panel shows the error in the refractive indices and the right panel shows the relative error in the thicknesses. It can be seen that the error of index extraction is insensitive to the sample's thickness profile. Our tests have also shown the same behavior when d_2 is fixed and d_1 is swept.

4 Discussion

So far, we have discussed only the ideal situation, where the actual optical path lengths are known exactly, where Eq. (6) could be solved for any wavenumber components as long as the determinant of the matrix is not zero. However, in practice, there is always an uncertainty (ϵ) associated with the measured optical path (δ'), so

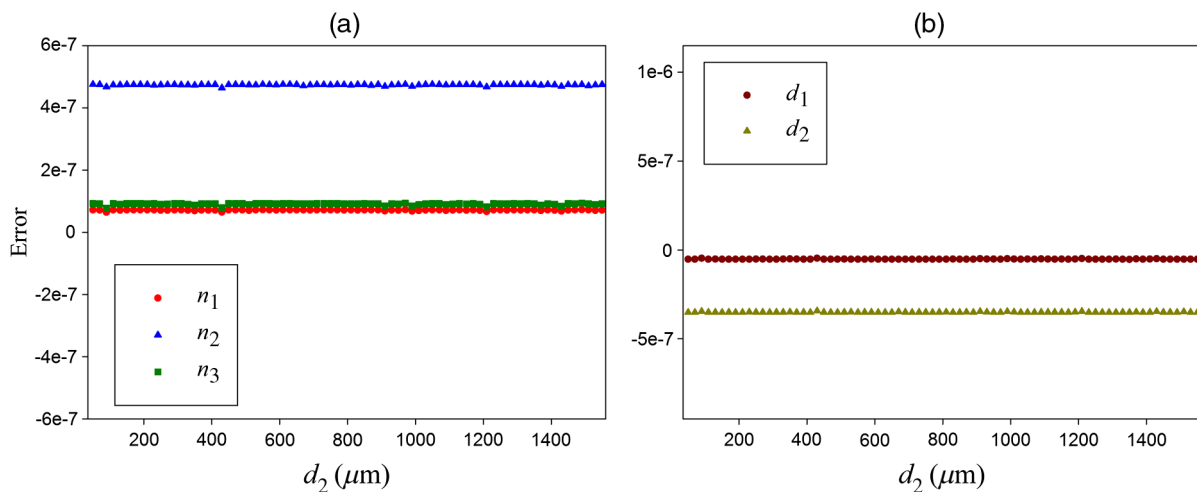


Fig. 3 Impact of sample thickness (varying d_2) on the accuracy of the sample's extracted parameters. (a) The errors associated with the refractive indices are shown, and (b) the relative error associated in the thicknesses is shown.

the value input into the parameter extraction algorithm may deviate from the actual optical path (δ) so that

$$\delta' = \delta \pm \varepsilon. \quad (13)$$

Since in practice, the matrix in Eq. (6) is constructed from the measured optical path lengths, there is a nonlinear phase shift between the matrix and the signal on the right-hand side of Eq. (6). Therefore, in the presence of ε , there will be a constraint on wavenumber selection in addition to the roots of the determinant and inappropriate selection of the wavenumber components can lead to significant errors. Given that this matrix equation presents a coupled set of transcendental equations containing index terms on both sides of the equal signs, the impact of ε on index determination is not transparent so the behavior of the extracted parameters is best investigated by simulation. A framework for selecting the suitable spectral components is investigated in the following section.

4.1 Finding a Suitable Set of Wavenumber Components

We illustrate the impact of the optical path length measurement error on the efficacy of parameter extraction using the following randomly selected two-layer system with indices $n_0 = 1.337$, $n_1 = 1.345$, $n_2 = 1.351$, and $n_3 = 1.337$ and thicknesses $d_1 = 10 \mu\text{m}$ and $d_2 = 30 \mu\text{m}$ and assuming that $\Delta_{z_R z_0} = 0$. Errors of $\varepsilon_1 = +3.0 \text{ nm}$ for the first layer and $\varepsilon_2 = +10.0 \text{ nm}$ for the second layer are arbitrarily introduced, to mimic the optical path length measurement error. Although the variation of the errors with $\varepsilon > 0$ and $\varepsilon < 0$ is not symmetric, our tests have shown that the whole discussion with $\varepsilon > 0$ is also valid for $\varepsilon < 0$. In order to solve Eq. (6), three spectral components are needed (k_1, k_2, k_3). We fix k_1 and k_2 at two arbitrary values [$k_1 = 6.80 (\mu\text{m})^{-1}$, $k_2 = 6.85 (\mu\text{m})^{-1}$] and sweep k_3 [from 6.85 to $7.00 (\mu\text{m})^{-1}$] to investigate the behavior of the extraction algorithm. The errors in extracting refractive indices are shown in Fig. 4, where the left vertical axis is the error in

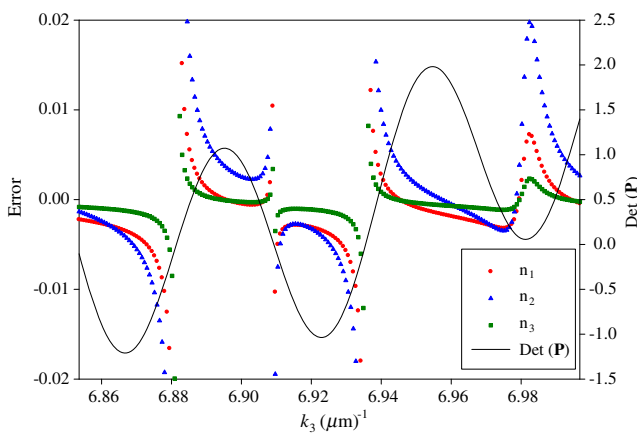


Fig. 4 The dependence of the extracted refractive indices errors as a function of the third wavenumber. The left axis shows error, and the right axis shows the determinant value. Two of the wavenumbers are chosen at arbitrary values and the third (k_3) is scanned. In this illustrative example, $n_0 = 1.337$, $n_1 = 1.345$, $n_2 = 1.351$, $n_3 = 1.337$, $d_1 = 10 \mu\text{m}$, and $d_2 = 30 \mu\text{m}$. The introduced error in OT is $\varepsilon_1 = +3.0 \text{ nm}$ for the first layer and $\varepsilon_2 = +10.0 \text{ nm}$ for the second layer. The chosen wavenumbers are $k_1 = 6.80 (\mu\text{m})^{-1}$, $k_2 = 6.85 (\mu\text{m})^{-1}$, and k_3 swept from 6.85 to $7.00 (\mu\text{m})^{-1}$.

the extracted indices, the horizontal axis is k_3 , and the second axis is the plot of the determinant of P.

From Fig. 4, it is seen that the errors in extracting indices vary with wavenumber. The figure also shows that the errors diverge where the determinant is zero and converge around the determinant's extrema. In fact, better convergence is observed with a larger magnitude of the determinant. This is a systematic behavior of the extracted parameter errors with respect to the wavenumber components and has been observed throughout our large number of tests. Since the determinant value solely depends on the chosen set of the spectral components, we may conclude from the observation in Fig. 4, that in order to reduce (if not minimize) the error of all the extracted parameters, we may look for a set of wavenumbers (k_1, k_2, k_3) that provides large magnitude (if not maximizes) of the determinant.

According to Hadamard's maximum determinant problem,⁵⁰ the formal maximum of the 3×3 matrix presented in Eq. (7) with all entries on the closed unit disk is $3^{3/2} = 5.196$. Since the formal approach to maximize the determinant of the matrix is too complicated and out of the scope of this article, we use a heuristic search to find a special set out of many possible sets. Thereby, it may not be the optimal selection but as we will show below it provides excellent estimates of the index parameters. Using the approach described in reference,⁴⁹ a set of possible wavenumber components for the example case mentioned above is $k_1 = 6.52 (\mu\text{m})^{-1}$, $k_2 = 8.52 (\mu\text{m})^{-1}$, and $k_3 = 8.64 (\mu\text{m})^{-1}$, which generate a determinant of 3.977. In order to show the behavior of the extracted indices errors with the new set of wavenumbers, we fix k_1 and k_2 at the given values above and sweep k_3 from 8.52 to $8.67 (\mu\text{m})^{-1}$ and plot the extracted indices errors versus wavenumber (Fig. 5). The determinant of the matrix is also plotted as a reference in the figure (the right axis).

It can be observed from Fig. 5 that the errors are reduced simultaneously around the maximum of the determinant (indicated

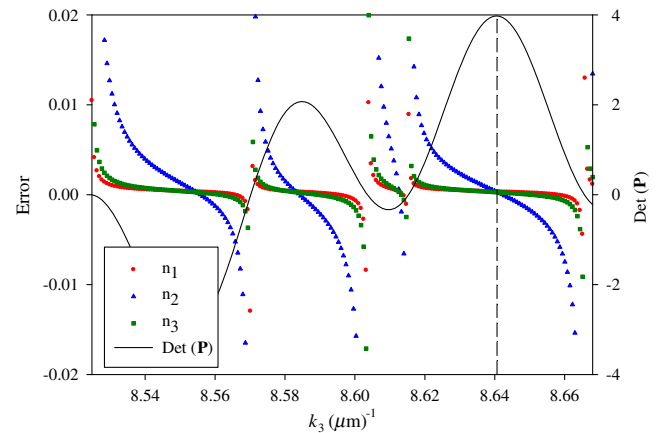


Fig. 5 The dependence of the extracted refractive index errors as a function of wavenumber selection for a two-layer system. The left axis is for refractive index error, and the right axis shows the determinant value. The wavenumbers are obtained from the algorithm that maximizes the determinant. In this illustrative example, $n_0 = 1.337$, $n_1 = 1.345$, $n_2 = 1.351$, $n_3 = 1.337$, $d_1 = 10 \mu\text{m}$ and $d_2 = 30 \mu\text{m}$. The introduced error in OT is $\varepsilon_1 = +3.0 \text{ nm}$ for the first layer and $\varepsilon_2 = +10.0 \text{ nm}$ for the second layer. The chosen wavenumbers are $k_1 = 6.52 (\mu\text{m})^{-1}$, $k_2 = 8.52 (\mu\text{m})^{-1}$ and k_3 swept from 8.52 to $8.67 (\mu\text{m})^{-1}$. The indicator line corresponds to $k_3 = 8.64 (\mu\text{m})^{-1}$ obtained from the algorithm.

by a dashed line on Fig. 5). The errors at the determinant's maximum are $n_1^{\text{actual}} - n_1^{\text{extracted}} = 3.23 \times 10^{-4}$, $n_2^{\text{actual}} - n_2^{\text{extracted}} = 2.98 \times 10^{-4}$, $n_3^{\text{actual}} - n_3^{\text{extracted}} = 2.79 \times 10^{-4}$, and for thicknesses after dividing the optical path length by the corresponding index of refraction, we obtain $d_1^{\text{actual}} - d_1^{\text{extracted}} = -4.62 \times 10^{-3} \mu\text{m}$ and $d_2^{\text{actual}} - d_2^{\text{extracted}} = -1.39 \times 10^{-2} \mu\text{m}$.

5 Conclusion

In conclusion, we introduced in this article a new framework for simultaneous extraction of refractive index and thickness of multilayer systems, from its FD-OCT data, without any previous information about the item under investigation. No additional arrangement, reference reflector, or mechanical scanning is needed, which is the main advantage of this approach.

In this method, the accuracy of the extracted parameters depends on the refractive index contrast of the object and is insensitive to thickness profile. The index contrast limitation is due to inherent differences between the modeled and actual spectrum. Our theoretical model takes into account only single scattering events, but the actual spectrum contains multiple scattering events. We showed in Sec. 3.1 that in biological applications, when $n_{1,2} \leq 1.55$, two-layer systems indices can be extracted with the absolute error ≤ 0.001 . This implies that the maximum tolerable index contrast is in the range of $|1.55 - 1.337| = 0.233$. This limitation is not a problem for the biological system, where the refractive index rarely exceeds 1.45.

We showed in this article that the uncertainty in measuring the optical path lengths (ϵ) has a significant impact on the extracted parameter errors. Two main questions arising here are what is the maximum ϵ that still allows extraction of parameters and how much is the accuracy loss in each parameter as ϵ increases. The impact of large amounts of ϵ , which may occur in practice, is discussed in part 2 of this article. Also, the proposed methodology for selecting the best spectral components in Sec. 4.1 is based on empirical examples and has not been proven to be the best methodology and needs to be validated through a proper theoretical work-up.

Disclosures

The authors have no relevant financial interests in the manuscript and no other potential conflicts of interest to disclose.

Acknowledgments

The authors would like to thank members of the PTC Community, Programming and Extending Mathcad online forum for their advice on simulation and programming techniques.

References

- W. Drexler and J. G. Fujimoto, Eds., *Optical Coherence Tomography*, Springer, Berlin, Heidelberg (2008).
- D. Huang et al., "Optical coherence tomography," *Science* **254**(5035), 1178–1181 (1991).
- A. F. Fercher et al., "Measurement of intraocular distances by backscattering spectral interferometry," *Opt. Commun.* **117**, 43–48 (1995).
- R. Leitgeb, C. Hitzenberger, and A. Fercher, "Performance of Fourier domain vs time domain optical coherence tomography," *Opt. Express* **11**(8), 889 (2003).
- M. Choma et al., "Sensitivity advantage of swept source and Fourier domain optical coherence tomography," *Opt. Express* **11**(18), 2183 (2003).
- J. F. de Boer et al., "Improved signal-to-noise ratio in spectral-domain compared with time-domain optical coherence tomography," *Opt. Lett.* **28**(21), 2067 (2003).
- Z. Wang et al., "Tissue refractive index as marker of disease," *J. Biomed. Opt.* **16**(11), 116017 (2011).
- Y. L. Kim et al., "Variation of corneal refractive index with hydration," *Phys. Med. Biol.* **49**(5), 859–868 (2004).
- M. A. Mayer et al., "Retinal nerve fiber layer segmentation on FD-OCT scans of normal subjects and glaucoma patients," *Biomed. Opt. Express* **1**(5), 1358–1383 (2010).
- S. J. Chiu et al., "Kernel regression based segmentation of optical coherence tomography images with diabetic macular edema," *Biomed. Opt. Express* **6**(4), 1172–1194 (2015).
- T. Garcia et al., "Optical coherence tomography in neuro-ophthalmology," in *Optical Coherence Tomography*, M. Kawasaki, Ed., pp. 77–100, InTech, Vienna, Austria (2013).
- B. Vuong et al., "Measuring the optical characteristics of medulloblastoma with optical coherence tomography," *Biomed. Opt. Express* **6**(4), 1487 (2015).
- F. A. South et al., "Differentiation of ex vivo human breast tissue using polarization-sensitive optical coherence tomography," *Biomed. Opt. Express* **5**(10), 3417 (2014).
- W. V. Sorin and D. F. Gray, "Simultaneous thickness and group index measurement using optical low-coherence reflectometry," *IEEE Photonics Technol. Lett.* **4**(1), 105–107 (1992).
- K. Watanabe, M. Ohshima, and T. Nomura, "Simultaneous measurement of refractive index and thickness distributions using low-coherence digital holography and vertical scanning," *J. Opt.* **16**(4), 45403 (2014).
- H.-C. Cheng and Y.-C. Liu, "Simultaneous measurement of group refractive index and thickness of optical samples using optical coherence tomography," *Appl. Opt.* **49**(5), 790 (2010).
- C.-T. Yen et al., "Simultaneously measuring the refractive index and thickness of an optical sample by using improved fiber-based optical coherence tomography," *Opt. Eng.* **53**(4), 044108 (2014).
- Y.-P. Wang et al., "Reflectometry measuring refractive index and thickness of polymer samples simultaneously," *J. Mod. Opt.* **53**(13), 1845–1851 (2006).
- G. J. Tearney et al., "Determination of the refractive index of highly scattering human tissue by optical coherence tomography," *Opt. Lett.* **20**(21), 2258 (1995).
- M. Ohmi et al., "Simultaneous measurement of refractive index and thickness of transparent plates by low coherence interferometry," *Opt. Rev.* **4**(4), 507–515 (1997).
- M. Ohmi et al., "In vitro simultaneous measurement of refractive index and thickness of biological tissue by the low coherence interferometry," *IEEE Trans. Biomed. Eng.* **47**(9), 1266–1270 (2000).
- M. Haruna et al., "Simultaneous measurement of the phase and group indices and the thickness of transparent plates by low-coherence interferometry," *Opt. Lett.* **23**(12), 966 (1998).
- H. Maruyama et al., "Low-coherence interferometer system for the simultaneous measurement of refractive index and thickness," *Appl. Opt.* **41**(7), 1315 (2002).
- T. Fukano and I. Yamaguchi, "Separation of measurement of the refractive index and the geometrical thickness by use of a wavelength-scanning interferometer with a confocal microscope," *Appl. Opt.* **38**(19), 4065 (1999).
- S. Kim et al., "Simultaneous measurement of refractive index and thickness by combining low-coherence interferometry and confocal optics," *Opt. Express* **16**(8), 5516 (2008).
- H. Maruyama et al., "Simultaneous measurement of refractive index and thickness by low coherence interferometry considering chromatic dispersion of index," *Opt. Rev.* **7**(5), 468–472 (2000).
- M. Ohmi et al., "High-speed simultaneous measurement of refractive index and thickness of transparent plates by low-coherence interferometry and confocal optics," *Meas. Sci. Technol.* **15**(8), 1531–1535 (2004).
- T. Fukano and I. Yamaguchi, "Simultaneous measurement of thicknesses and refractive indices of multiple layers by a low-coherence confocal interference microscope," *Opt. Lett.* **21**(23), 1942 (1996).
- X. Wang et al., "Simultaneous refractive index and thickness measurements of bio tissue by optical coherence tomography," *J. Biomed. Opt.* **7**(4), 628–632 (2002).

30. S. A. Alexandrov et al., "Bifocal optical coherence refractometry of turbid media," *Opt. Lett.* **28**(2), 117–119 (2003).
31. A. Zvyagin et al., "Refractive index tomography of turbid media by bifocal optical coherence refractometry," *Opt. Express* **11**(25), 3503–3517 (2003).
32. G. Min, J. W. Kim, and B.-H. Lee, "The refractive index measurement technique based on the defocus correction method in full-field optical coherence tomography," *Proc. SPIE* **8428**, 84281M (2012).
33. G. Min et al., "Refractive index measurements of multiple layers using numerical refocusing in FF-OCT," *Opt. Express* **21**(24), 29955–29967 (2013).
34. H. Matsumoto, K. Sasaki, and A. Hirai, "In situ measurement of group refractive index using tandem low-coherence interferometer," *Opt. Commun.* **266**(1), 214–217 (2006).
35. A. Hirai and H. Matsumoto, "Low-coherence tandem interferometer for measurement of group refractive index without knowledge of the thickness of the test sample," *Opt. Lett.* **28**(21), 2112–2114 (2003).
36. D. F. Murphy and D. A. Flavin, "Dispersion-insensitive measurement of thickness and group refractive index by low-coherence interferometry," *Appl. Opt.* **39**(25), 4607 (2000).
37. J. Jin et al., "Thickness and refractive index measurement of a silicon wafer based on an optical comb," *Opt. Express* **18**(17), 18339–18346 (2010).
38. J. Na et al., "Self-referenced spectral interferometry for simultaneous measurements of thickness and refractive index," *Appl. Opt.* **48**(13), 2461 (2009).
39. Y.-S. Ghim and S.-W. Kim, "Thin-film thickness profile and its refractive index measurements by dispersive white-light interferometry," *Opt. Express* **14**(24), 11885 (2006).
40. S. J. Park et al., "Simultaneous measurements of refractive index and thickness by spectral-domain low coherence interferometry having dual sample probes," *IEEE Photonics Technol. Lett.* **23**(15), 1076–1078 (2011).
41. P. H. Tomlins and R. K. Wang, "Simultaneous analysis of refractive index and physical thickness by Fourier domain optical coherence tomography," *IEE Proc. Optoelectron.* **153**(5), 222 (2006).
42. T. Lai and S. Tang, "Cornea characterization using a combined multiphoton microscopy and optical coherence tomography system," *Biomed. Opt. Express* **5**(5), 1494 (2014).
43. Y. Zhou et al., "Characterizing refractive index and thickness of biological tissues using combined multiphoton microscopy and optical coherence tomography," *Biomed. Opt. Express* **4**(1), 38–50 (2012).
44. A. Knüttel and M. Boehlau-Godau, "Spatially confined and temporally resolved refractive index and scattering evaluation in human skin performed with optical coherence tomography," *J. Biomed. Opt.* **5**(1), 83–92 (2000).
45. P. H. Tomlins and R. K. Wang, "Matrix approach to quantitative refractive index analysis by Fourier domain optical coherence tomography," *J. Opt. Soc. Am. A* **23**(8), 1897 (2006).
46. P. H. Tomlins and R. K. Wang, "Layer dependent refractive index measurement by Fourier domain optical coherence tomography," *Proc. SPIE* **6079**, 607913 (2006).
47. J. A. Izatt and M. A. Choma, "Theory of optical coherence tomography," in *Optical Coherence Tomography*, P. D. W. Drexler and P. D. J. G. Fujimoto, Eds., pp. 47–72, Springer, Berlin, Heidelberg (2008).
48. M. Wojtkowski et al., "Full range complex spectral optical coherence tomography technique in eye imaging," *Opt. Lett.* **27**(16), 1415 (2002).
49. P. Rajai, "Measurement of refractive index and thickness of multilayer systems using Fourier domain optical coherence tomography," MS Thesis [PhD Thesis], University of Ottawa (2016).
50. E. W. Weisstein, "Hadamard's maximum determinant problem," 2017, <http://mathworld.wolfram.com/HadamardsMaximumDeterminantProblem.html> (18 November 2015).

Payman Rajai obtained his bachelor and master's degrees in applied physics from Islamic Azad University, Tehran, Iran in 1995 and 2000 respectively, and his PhD in physics from the University of Ottawa in 2016. He has also spent over 10 years in the contact lens manufacturing industry.

Henry Schriemer received his PhD in physics from the University of Manitoba in 1997. He is an associate professor in electrical engineering at the University of Ottawa, where he previously held an NCIT research fellowship in photonics after spending several years in the photonics industry. Other recent activities have ranged across the photovoltaics landscape, with a present focus on energy management for smart grids. He has authored over 90 peer-reviewed publications.

Ahmad Amjadi received his master and PhD degree from Michigan State University in 1982 and 1986 respectively. Now he is associate professor in the physics department of Sharif University of technology, Tehran, Iran and head of Sharif Applied Physics Research Center since 2003. His research interest is medical physics especially application of laser in medical research.

Rejean Munger received his MSc and PhD degrees from Physics Department, the University of Waterloo, Ontario, Canada, in 1986 and 1990, respectively. He was a lecturer and research associate at the School of Optometry of the University of Waterloo from 1989 to 1994 and a research associate at the National Research Council Canada from 1994 to 1996. He then joined the University of Ottawa Eye Institute doing biomedical photonic research until 2013. He has since focused on the development of several startup biomedical photonic ventures.